Molecular Crystals and Liquid Crystals

ISSN: 1542-1406 (Print) 1563-5287 (Online) Journal homepage: http://www.tandfonline.com/loi/gmcl20

Anomalous Scaling, Intermittency and Turbulence in Nematic Liquid Crystals

F. Carbone, F. Ciuchi, A. Mazzulla & L. Sorriso-Valvo

To cite this article: F. Carbone, F. Ciuchi, A. Mazzulla & L. Sorriso-Valvo (2015) Anomalous Scaling, Intermittency and Turbulence in Nematic Liquid Crystals, Molecular Crystals and Liquid Crystals, 614:1, 67-85, DOI: 10.1080/15421406.2015.1049911

To link to this article: http://dx.doi.org/10.1080/15421406.2015.1049911

Published online: 18 Aug 2015.

Mol. Cryst. Liq. Cryst., Vol. 614: pp. 67–85, 2015

ISSN: 1542-1406 print/1563-5287 online
DOI: 10.1080/15421406.2015.1049911

Anomalous Scaling, Intermittency and Turbulence in Nematic Liquid Crystals

F. CARBONE,[1,*] F. CIUCHI,[2] A. MAZZULLA,[2,*] AND L. SORRISO-VALVO[2]

[1]CNR IIA, U.O.S. Rende c/o University of Calabria Polifunzionale Rende (CS), Italy
[2]CNR Licryl c/o Physics Dept. University of Calabria and Excellence Centre CEMIF.CAL, Rende (CS), Italy

Turbulent electro-convective fluctuations induced in nematic liquid crystal (NLC) by an external oscillating electric field application are studied. Electrohydrodinamic instabilities, including chaotic dynamics and irregular pattern formation, are induced by electrical forces coupled to the flow, the conductivity and the bulk forces acting on the volume charges. In particular we investigate the scaling behavior of the probability density function (PDFs) of intensity fluctuations in a NLC driven through different regimes far from the cell plates, by using the confocal fluorescence microscopy technique. Both spectral properties and scaling behavior of light intensity fluctuations PDFs are analysed at different voltages. In weak turbulent regime, for intermediate voltages, PDFs are Gaussian at large scales, while show enhanced wings at smaller scales, showing the typical intermittency of the isotropic fluid flows. At higher voltages complex dynamical scattering regimes take place. A quantitative estimation of intermittency is obtained by PDFs modeling through the Castaing distribution, and structure functions are calculated in the framework of Extended Self-Similarity. Generation of small-scale fluctuations through a fragmentation process of large-scale structures are supported by the results. Moreover, the lingering anisotropic properties of the fluctuations are highlighted by the outcomes.

Keywords liquid crystals; hydrodynamics; statistical physics and nonlinear dynamics; Turbulent flows

Introduction

The turbulence in fluid flows is known to generate high amplitude fluctuations on all dynamical spatial and temporal scales, giving rise to scale free relationships for statistical quantities [1–3]. On the basis of experimental results [4–7] and numerical simulations [8, 9], it has been long accepted that scaling behaviours are anomalous with respect to the Kolmogorov phenomenology [10, 3]. This seems to be a universal characteristic of turbulent flows, being observed also in complex fluids, such as turbulent astrophysical [11–13] and

*Address correspondence to F. Carbone and A. Mazzulla, CNR IIA, U.O.S. Rende c/o University of Calabria Polifunzionale 87036 Rende (CS), Italy; CNR Licryl c/o Physics Dept. University of Calabria and Excellence Centre CEMIF.CAL, 87036 Rende (CS), Italy. E-mail: francesco.carbone@fis.unical.it, alfredo.mazzulla@cnr.it

Color versions of one or more of the figures in the article can be found online at www.tandfonline.com/gmcl.

charged particle flows [14, 15]. The process leading to anomalous scaling is usually called intermittency [10].

The name "intermittency" may refer to different aspects of turbulent flows. Here we deal with small scale intermittency, usually associated with the tendency toward spatial and temporal localization of the small scale structures of turbulent flows.

The signature of small-scale intermittency is the lack of global self-similarity, as evidenced, for example, by the scaling behaviour of probability density function (PDF) of fluctuations. In fact, PDFs of field increments across the scale $r$change shape with the scale, evolving from quasi-Gaussian at large scales, to stretched exponential distribution at small scales. In fluid flows, this has been associated with the inhomogeneous distribution of turbulent energy dissipation rate [10]. In complex fluid flows, dissipation properties can be significantly different from usual fluids, so that the presence of intermittency can also be due to structures associated with large local gradients [11–15].

Many experimental results [16–19] have shown that deviation from a Kolmogorov-like phenomenology can be stronger in anisotropic flows [20].

Nematic liquid crystals (NLC) represent an interesting class of anisotropic fluids displaying complex spatio-temporal behavior [21, 22]. NLC are particularly suitable for experimental study.

Indeed, dynamical patterns and flows can be easily observed, since the distortion of the molecular field produce a modulation in the refraction index, with direct effect on the light transmission. Moreover, several control parameters (such as external fields or external stress) can be tuned to explore different conditions and study regime transitions.

NLC are usually made of long anisotropic molecules, with properties characterized by a single anisotropy axis known as molecular director $n(r)$. The dielectric tensor can be written as $\varepsilon_{ij} = \varepsilon_0\delta_{ij} + \Delta\varepsilon n_i n_j$, where $\Delta\varepsilon$ is the dielectric anisotropy of the material ($\Delta\varepsilon \equiv \varepsilon_{||} - \varepsilon_{\perp}$) and$\delta_{ij}$ is the usual Kronecker delta.

When a NLC sample is stimulated by an external electric field, electrical forces may couple to the flow. Moreover, charge conduction can play an important role, together with bulk forces acting on the volume charge buildup. These effects lead to electrohydrodynamic instabilities (EHD) driven by electrical forces [21, 22]. Therefore, spatio-temporal chaotic dynamics and formation of irregular patterns can be observed in NLC, and can be studied by tuning the amplitude of the external field.

Although weakly nonlinear regimes of EHD have been successfully studied in the past [21–25], the nonlinear behaviour arising at large external field amplitudes still lacks a satisfactory description.

Recent experimental results have suggested the possible analogy between nonlinear EHD regimes and the turbulent motion of fluids [26–31]. Such analogy has also been supported by the phenomenological description of EHD through the Navier-Stokes equations coupled with Maxwell equations [30].

In this work we make use of data analysis tools for the experimental description of electroconvective dynamics of NLC. In particular we investigate the scaling behavior of the PDFs of intensity fluctuations in a NLC driven through different regimes far from the plates of the traditional liquid crystal cell, by using the confocal fluorescence microscopy technique.

Experimental Setup and System Description

The sample studied in this work consists of a planar cell of [N-(4-Methoxybenzyliden)-4-butylanilin] (MBBA) NLC at controled room temperature of 20 deg C, with thickness

$L_z = 50\ \mu m$. An oscillating electric field $E = (0, 0, E_z)$, where $E_z = V_0/L_z$ and V_0 is an external tunable voltage, is applied to the sample plates.

In order to apply the electric field a Indium tin oxide (ITO) electrode of area $A \sim 1cm^2$ is deposed on the plates. Since MBBA has $\Delta\varepsilon < 0$, when the electric field is applied the molecular director tends to align $n \perp E$. In order to eliminate ion segregation, the field oscillation frequency is $f = 70\ Hz$, well below the critical frequency $f_c = 120\ Hz$, that establishes the transition point between the conductive and dielectric behaviors [21].

The cell plates are treated in order to favor the alignment of the director n in the direction y parallel to the plates. Thus, for $V_0 = 0$, the average director $\langle n \rangle$ is along the y direction ($n = (0, n_y, 0)$, and the liquid crystal is at rest. EHD instabilities develop when the external voltage V_0 exceeds a critical value, $V_c \sim 7.5V$ in the case under study.

The threshold voltage is approximately independent of the sample thickness, while it is affected by the concentration of ions and impurities.

In order to avoid boundary or electric coherence effects [21] in the flow, we analyzed the sample at a depth $z = 20\ \pm\ 1\mu m$, by doping the sample with a fluorescent dye (Pyrromethene 597 dye 0.3% wt), and then scanning it by a confocal fluorescence polarization microscope (Zeiss LSM-510) [26].

The dye molecules dissolved in the NLC are fully miscible at this concentration, as evidenced by the absence of micro clusters of dye embedded in the liquid crystalline phase [32, 33]. Confocal microscopes can acquire in-focus images from selected depths (a process known as optical sectioning), which allows a 3D tomography of topologically complex objects. Each pixel in the image represents the detected light emitted by a volume element within the sample, when the dye molecules are stimulated by a light source. A He-Ne laser (with wavelength $\lambda_L = 543\ nm$) linearly polarized along the y axis, was focused inside the sample with a high numerical aperture (NA = 1.40) objective lens, used as an optical pump. In this configuration the incident polarization $\mathbf{P}$ is parallel to the director n of the sample for $V_0 = 0$.

The thickness of the focal plane (vertical spatial resolution) is given by $\Delta Z \sim 1/(NA)^2$, whereas the in-plane spatial resolution is $\Delta X = \Delta Y \sim 1/NA$ [34, 35].

The focal point of the laser was scanned over the three-dimensional volume, and the fluorescence from each point was selectively detected by a photomultiplier tube behind a pinhole, placed at a confocal configuration. The anisotropic dye molecules easily align with the molecular director $n(x)$ and follow the internal flow of EHD instabilities [32, 33, 26]. In other words, the transition dipole of the dye molecules (for excitation and fluorescent emission) is parallel to the director n. As the laser is scanned over the plane of interest, a section image $I'(x)$ of the internal structure of the sample is acquired (see Figure 2).

The brightness of each pixel $I'(x)$ is proportional to the relative intensity of detected light. Due to larger light absorption of the dye molecules along its symmetry axis [32–35], and subsequent light emission, bright regions represent $I'(x)$ portions of volume in which the dye (and thus the NLC) molecules have their longer molecular axis parallel to the polarization of the incident laser beam ($\mathbf{P} \parallel n$).

If n is perpendicular to the incident polarization ($\mathbf{P} \perp n$) the intensity $I'(x)$ is minimum. For an angle $0 \leq \theta \leq \pi/2$ between the director n (or the dipole moment of the dye molecules) and the incident polarization $\mathbf{P}$ the detected intensity $I'(x) \sim \cos^4\theta$. Therefore an intensity map acquired with the incident polarization $\mathbf{P}$ along the y axis is proportional to n_y^4 [36], where n_y is the y-component of the director n, which in turn is dynamically coupled to the liquid crystal flow [37–40].

EHD instabilities have been investigated for a long time. It has been shown that the system can be forced out of equilibrium for voltages slightly above the critical value, $V_0 = V_c + \Delta V$. In order to compare different experiments with different sample geometries

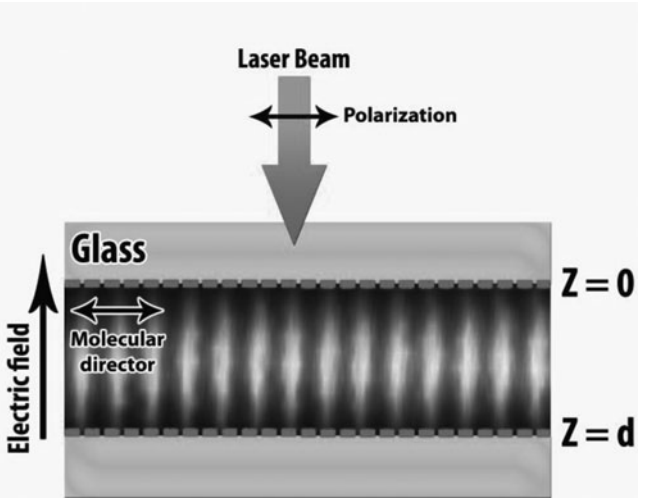

Figure 1. A snapshot of the y, z plane for $\varepsilon^I = 0.21$, representing the geometry of the system. The high intensity zone represents the convective structures occurring in the WD. In these zone the molecular axis is parallel to the incident polarization.

or aspect ratio, it is customary to introduce the reduced parameter $\varepsilon^I = (V_0^2 - V_c^2)/V_c^2$, which represents the normalized deviation from the critical voltage.

The first instability setting up above the critical voltage consists of a spatially periodic pattern of convective rolls, whose axis is normal to the y direction and whose periodicity is of the order of L_z.

Assuming that the electrodes inject charges inside the sample, under the action of the electric field the charged NLC layer will be pushed up against the counteracting gravity force. For energetic reason, the charge layer will not move as an entire block but it will rather be fragmented into cylindrical vortices along the z direction (figs. 1 and 2) [21, 22]. The fragmentation results in a periodic distribution of charges on the $x - y$ plane, so that the periodic flow will inevitably interact with the NLC director n. The deflection of n in the z direction can be observed where the molecular shear rate is maximum (i.e. in the middle of the vortices). On the other hand, the fluid velocity is maximum between vortices, where the space charge is accumulated.

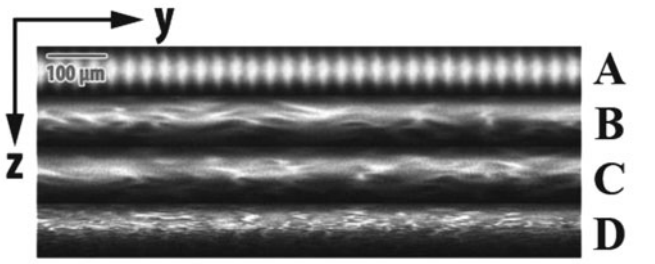

Figure 2. Same as figure 1, y, z profile of sample encoded with fluorescent dye PM597 0.3% wt, for different ε^I : A) $\varepsilon^I = 0.21$, B) $\varepsilon^I = 9.89$, C) $\varepsilon^I = 15$, D) $\varepsilon^I = 52.29$.

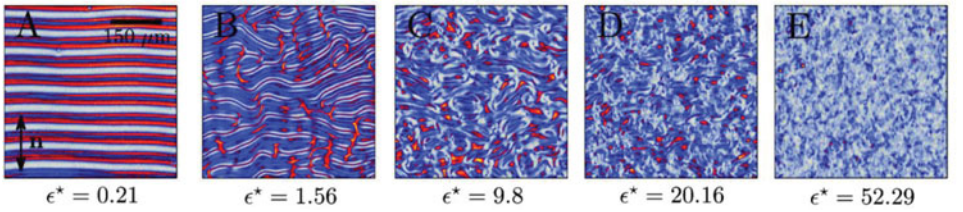

Figure 3. Snapshots of the light intensity field for five different values of ε^* (arbitrary color scale). (A): Williams Domains; (B): fragmented WD; (C) weak turbulence regime; (D): strong turbulence DSM1 regime; (E): strong turbulence DSM2 regime.

The resulting patterns, resembling convective rolls, are called Williams Domains (WD) (fig. 3, panel *A*), and the regime share some qualitative analogies with the Rayleigh-Bénard instability in fluid flows [41]. Importantly, the emergence of the regular pattern of well aligned convective rolls introduces anisotropy in the system, so that the WD axis represents a relevant anisotropy direction.

Since the electrical forces can be much stronger than the gravitational buoyancy, the characteristics length and time scales of EHD are typically much shorter than in the fluid case. This allows the experimental study of very large aspect ratio systems than in the fluid case.

After the setup of the convective instability the voltage is increased to explore more complex regimes. Indeed, as ε^I increases, the system continuously undergoes a sequence of different bifurcations, with spatio-temporal states with increased disorder (fig. 2). Note that the transitions between regimes are smooth, without a threshold values.

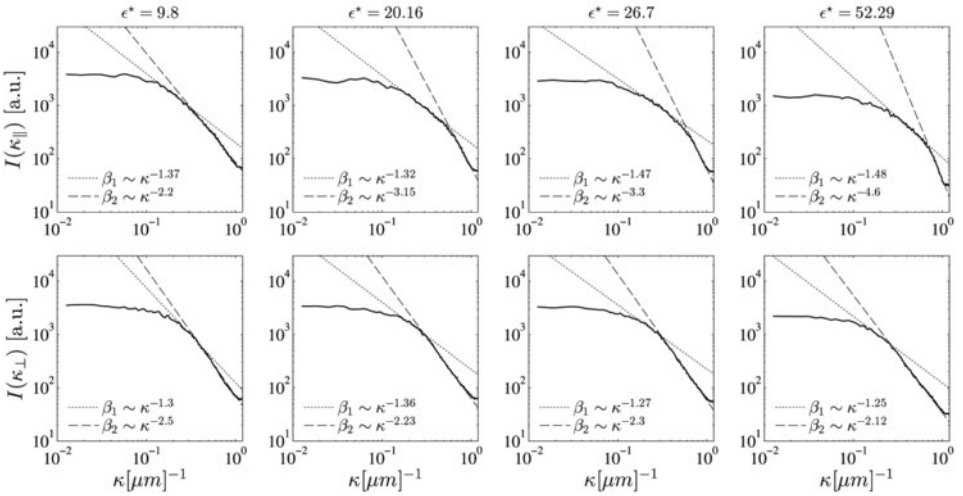

Figure 4. The directional power spectra of the light intensity field, for wavevectors parallel (top panels) and perpendicular (bottom panels) to the WD axis. The four columns refer to four different values of ε^I (see titles). Power law fits are indicated as dotted (larger scales) and dashed (smaller scales) lines. The spectral indices obtained though least-square fits in the appropriate ranges are indicated in each panel.

For $\varepsilon^I \sim 0.3$ the formation of defects in the WD pattern is observed. For higher values, the WD reduce their size and begin to fragment (fig. 3, panel B). By increasing the control parameter ε^I, the characteristic time and space scales continuously decrease, until the system reaches a chaotic state, with the formation of small scale structures (fig. 3, panel C), referred to as weak turbulence regime. In this regime, the NLC flow field can be considered as a superposition of elementary convective structures randomly distributed in space and fluctuating in time. Such structures appear as a randomly moving ensemble of small domains, characterized by patterns on all spatial scales [26, 27, 42].

For higher values of ε^I, after the sequence of bifurcations, the sample reaches a strongly chaotic regime, traditionally called Dynamic Scattering Mode (DSM) (fig.3, panel$D$). Two different kinds of DSM have been observed, DSM1 and DSM2. The DSM2 state (fig. 3, panel$E$) sets up at larger voltage, and the transition $DSM1 \rightarrow DSM2$ takes place as nucleation of small areas of DSM2 type within the DSM1 state, and their subsequent expansion. It has been recently suggested that this transition ($DSM1 \rightarrow DSM2$) acts as an absorbing phase transition between the active DSM2 phase and the absorbing DSM1 phase [43]. At $\varepsilon^I = 52.29$ (fig. 3, panel E), the sample has fully evolved into the DSM2 regime.

It should be pointed out that the anisotropy induced by the presence of the WD at low voltage, is persistent and has effects on the statistical properties of the more chaotic regimes at larger voltage, even after the convective rolls have been completely apparently fragmented in small scale structures [27, 28].

Spectral Properties and Scaling of the Probability Distribution Functions of Intensity Fluctuations

As is customary in turbulence studies, important information on the nature of the fields fluctuations can be inferred by observing the scaling properties of the power spectral density $I(\kappa_\alpha)$ [3]. Here κ_α represents the wave vectors in the directions parallel ($\alpha = \|$) or perpendicular ($\alpha = \perp$) to the WD axis, which is the main anisotropy direction in our experiment. The choice of performing separate analysis for parallel and perpendicular fluctuations is driven by the persistence of anisotropy in the chaotic regimes [27, 28].

Figure 4 shows the directional spectra of the light intensity field for the five snapshots depicted in top panels of the same figure, in different EHD regimes. At low voltage (corresponding to panel A), the signature of the WD is evident as spikes of the parallel spectrum, while the perpendicular spectrum is noise-dominated.

As ε^I (and therefore the complexity of the patterns) increases, the spectra evolve toward a power-law decay $I(\kappa_\alpha) \propto \kappa_\alpha^{-\beta}$ (β indicating the spectral index), which is similar to the typical behaviour observed in turbulent flows. This similarity is more evident starting from the weak turbulence regime (upper panel, column 3 of fig. 4). From now on, we will focus our analysis on these regimes (weak turbulence and the two DSM regimes, panels C, D and E of figure 4), where similarities with turbulence are evidenced by the spectral shape.

The spectral index β can be obtained through a least-square fit of the spectra to power-laws, as shown from the superimposed dashed and dotted lines in figure 5. for four different values of ε^I in the chaotic regimes. In the intermediate range of wave vectors, the spectra are compatible with a Kolmogorov-like decay, with exponents around $\beta \sim 1.3 \div 1.5$, while at smaller scale a steeper spectrum is observed, typically with $\beta \sim 2 \div 4$. Persistent anisotropic effects are evident from the comparison of parallel and perpendicular spectra. In particular, note that for the perpendicular spectra the intermediate fitting range is very limited, so that the power-law fit is only indicative of a possible fragmentation process.

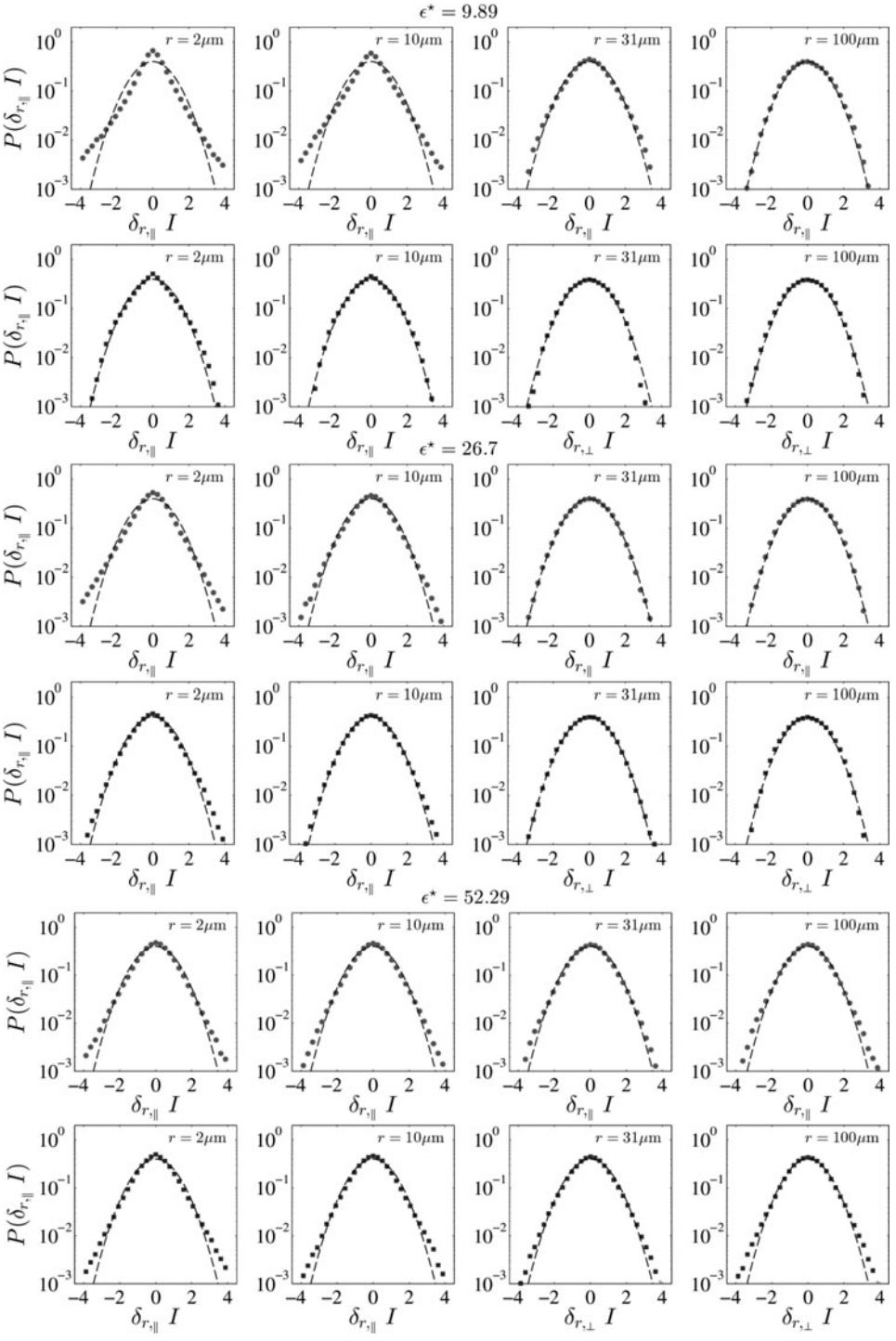

Figure 5. PDFs of the intensity fluctuations in the parallel and perpendicular directions, at different lags $\boldsymbol{r}$, and at three different values of ε^I indicated at the top of each set of panels. The dashed lines represent standard Gaussians.

In order to gain more detailed information about the system, it is customary to analyze the flow properties through the representation given by the field increments estimated at different lags r, which represent a probe for turbulent structures at a given scale.

Based on the qualitative similarity between fluid turbulence and EHD, in this article we will refer to our system as to a sample of EHD turbulence, keeping in mind that this does not imply the validity of the whole theoretical framework of fluid turbulence in EHD. Thus, we make use of the longitudinal ($\parallel$) and perpendicular ($\perp$) intensity fluctuations with respect to the direction of the original WD convective rolls axis (x, in our reference frame), which introduces anisotropy (1.1, 1.2):

$$\delta_{r,\perp} I'(x, y) = I'(x, y + r) - I'(x, y)$$
$$\delta_{r,\parallel} I'(x, y) = I'(x + r, y) - I'(x, y).$$

To get PDFs with zero average and unit standard deviation we use, as customary, the normalized fluctuation of the turbulent field:

$$\delta_{r,\alpha} I = \frac{\delta_{r,\alpha} I'}{\langle (\delta_{r,\alpha} I' - \langle \delta_{r,\alpha} I' \rangle)^2 \rangle^{1/2}}$$

where α represents again either the longitudinal ($\parallel$) or perpendicular ($\perp$) direction.

Such normalization is required in order to compare the shape of the PDFs at different scales. The normalized PDFs are evaluated using uniformly spaced bins. The scaling behavior of PDFs, for different values of ε^I, is shown in figure 5. Gaussian curves are superposed to the observed PDFs as reference (dashed lines).

PDFs of parallel fluctuations are roughly Gaussian at large scales, and show rising tails as the scale gets smaller and smaller. This indicates that at small scales strong fluctuations have higher probability of occurrence than Gaussian distributed random events. Thus, correlations exist, due to structures accumulation at small scales. This feature is closely similar to the effects of intermittency in fully developed turbulence [3, 44, 45], and could be related to the structure fragmentation process occurring as ε^I increases. In EHD, the structures cascading mechanism could arise from the fragmentation of the convective rolls, which provide the energy injection necessary for the Richardson cascade scenario [27].

A similar behaviour is found in the perpendicular direction, at least for higher voltage regimes: PDFs are roughly Gaussian at large scale, but deviation from Gaussian seems weaker than for the parallel case. Furthermore, at lower voltage (for $\varepsilon^I < 9.89$) the scale dependency is not yet observed, so that the onset of intermittency is slower in this direction.

In the DSM2 regime, at $\varepsilon^I = 52.29$, the PDFs of both parallel and perpendicular increments weaken the dependence on the scale, and are closer to the same (roughly exponential) distribution at all scales. This suggests that at high voltage, starting at the threshold value $\varepsilon^I = 52.29$, the nonlinear fragmentation process slows down, so that structures are found at all scales with similar probability (closer to self-similarity).

A Model for the Scaling of the PDFs

It is important to quantitatively describe the scaling properties of PDFs shown in figures 5. To this aim, following the spirit of this work, we will focus on a PDF model referred to as Castaing model, originally developed for fluid turbulence [44], and successfully applied in other contexts [46–50].

Within the multifractal framework [3], it can be assumed that different regions of space have different local energy transfer rates, resulting in the inhomogeneous and scale

dependent topology of the energy dissipation rate. The model PDF consists of a continuous superposition of PDFs of a given shape (to be determined as the large scale distribution P_0), each representing one particular subset of data, associated with regions with similar energy transfer rate. Each curve has a given width σ and weight, introduced through the distribution function of the variances [44]. This corresponds to evaluate the convolution:

$$P_{\lambda_r,\alpha} = \int_{-\infty}^{\infty} \mathcal{L}_{\lambda_r}(\sigma_r) P_0(\delta_{r,\alpha} I, \sigma_r)\, d\ \ln \sigma_r .$$

The distribution of variances $\mathcal{L}_{\lambda_r}(\sigma_r)$ has to be chosen according to some assumptions about the energy cascade. By analyzing figures 5, a Gaussian large scale distribution can be used (in a range $\varepsilon^I \in [9.8, 52.29]$). Furthermore, as can be conjectured in the framework of the $K62$ theory [51], a log-normal ansatz can be used for the distribution of variances [44]:

$$\mathcal{L}_{\lambda_r}(\sigma_r) = \frac{1}{\lambda_r \sqrt{2\pi}} \exp - \left[\frac{\ln^2 \sigma_r/\sigma_{0,r}}{2\lambda_r^2} \right].$$

In eq. (1.5), λ_r^2 is the variance of the $\ln \sigma_r$ distribution, and $\sigma_{0,r}$ is the most probable value of σ at scale r.

It is easy to see that for $\lambda_r^2 = 0$ the log-normal PDF reduces to a δ-function, so that the convolution (1.4) gives one Gaussian of width $\sigma_{0,r}$. As λ_r^2 increases, the convolution includes more and more different values of σ, so that the tails of the PDF raise.

The scaling behavior of the single parameter λ_r^2 describes the deviation from the large scale distribution and the shape of the PDF wings. Such parameter has been successfully used to characterize the intermittency.

In the inertial range of fully developed turbulence, a power-law scaling of the parameter λ_r^2 is often observed [44, 46]. Such scaling exponent has been linked to the multifractal properties of the flow [44]. Moreover, it is easy to show that if the large scale PDF is Gaussian, then a relationship exists between λ_r^2 and the kurtosis of the PDF [44], namely its weighted fourth order moment $K(r) = \langle \delta_r I^4 \rangle / \langle \delta_r I^2 \rangle^2$, customarily used to quantitatively estimate intermittency [3]:

$$K(r) = 3\sigma_{0,r}^4 \exp 4\lambda_b^2 r .$$

The original model described in [44] also includes the skewness parameter a_s, which is needed to take into account the asymmetries of the PDFs, typical of intermittent turbulence. In this work we have used the complete form of the model PDF.

The Castaing model has been used to fit the PDFs of our EHD dataset at each scale. Examples of fit are presented in figure 6 (dashed line superimposed to the pdfs) showing that the model very satisfactorily reproduces the scale evolution of the PDFs. The parameter λ_r^2 can therefore be used to describe the scaling properties of the fluctuations.

In Figure 7 is reported the scale dependence of λ_r^2 for parallel and perpendicular increments, for different values of the voltage. In the parallel direction (top panel) a power law scaling $\lambda_r^2 \propto r^{-\gamma}$ is observed. Such scaling exponents are very similar ($\gamma \simeq 0.7$) for all values of ε^I except the DSM2 regime, indicating that the multifractal properties of the cascade are similar at all such voltages [44], at least within a given range of scales.

Saturation of the multiplicative process is observed at small scales, and more precisely, for example, at $r \simeq 7\ \mu m$ for $\varepsilon^I = 9.8$ and $r \simeq 4\ \mu m$ for $\varepsilon^I = 20.16$. This confirms that the fragmentation process is more efficient and reaches smaller scales at higher voltages

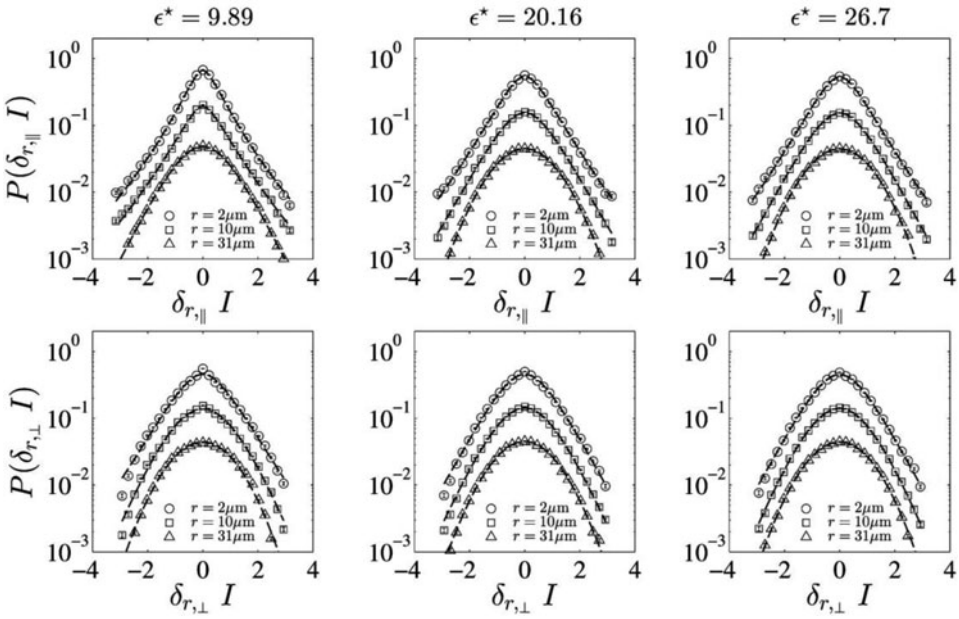

Figure 6. Intensity fluctuations PDFs at three different scales (see legend) for parallel and perpendicular increments, at three different increasing values of the voltage (from the left to the right). The fit with the Castaing model is superimposed (solid line). PDFs have been vertically shifted for clarity.

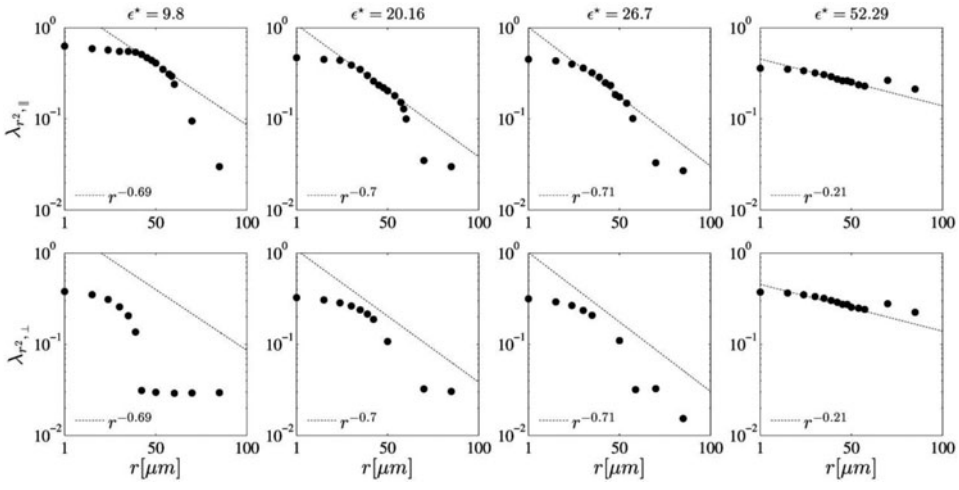

Figure 7. The scaling behaviour of the parameter λ_r^2 as obtained through fit with the Castaing model of the experimental PDFs of intensity fluctuations in the parallel (top panels) and perpendicular (bottom panels) directions. In the top panels, a power-law fit is also superimposed as dotted line, the corresponding scaling exponent being indicated in each plot. In the bottom panels, the dashed lines and the legends indicate the power-laws obtained for the parallel fluctuations (top panels), and are displayed in order to guide the eye.

(more developed turbulence). Small λ^2 values, corresponding to quasi-Gaussian PDFs, are observed at large scales.

In the DSM2 regime (top left panel of figure 6), the scaling of λ^2 changes dramatically, with a much shallower exponent ($\gamma \simeq 0.2$). In the Castaing picture, this corresponds to a larger fractal dimension of the typical structures, and to a smaller degree of multifractality and intermittency.

The power-law scaling is not evident for the perpendicular increments (bottom panel of figure 7), although the general behaviour (decrease toward larger scales) is similar to the parallel case. No strong difference can be pointed out between the different voltages preceding the DSM2 regime.

Vanishing values of the parameter, indicating decorrelation and no deviation from Gaussian statistics, are reached at scales smaller than in the parallel direction. Note that anisotropy of turbulent properties were also observed through the study of the spatio-temporal decorrelation [28].

In the DSM2 regime (bottom left panel of figure 7), the Castaing parameter scales with a more definite power-law, with identical exponent as for the parallel fluctuations. This seems to indicate isotropization of the sample, with a remarkable loss of memory of the WD symmetries.

In order to check the validity of the Castaing approach, in figure 8 we show the comparison between the kurtosis computed directly from data (open markers), and from the parameter λ_r^2 through eq. (1.6) (full markers). As usual, top panels refer to the parallel fluctuations, while bottom panels describe perpendicular fluctuations. Before the DSM2 regime, kurtosis of the parallel fluctuations is sensibly increasing from the large scale Gaussian value $K = 3$ toward smaller and smaller separation scales, indicating intermittency. This is less evident for the perpendicular fluctuations, where only at very small scales some weak increase of the kurtosis is observed. The two sets of values are in very good agreement with each other, with the possible exception of the very small scales in the DSM2 regime

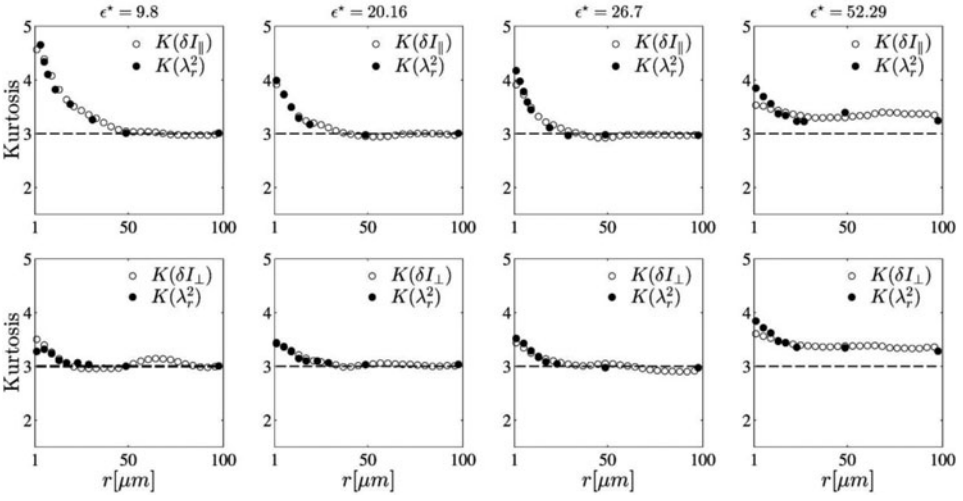

Figure 8. The scaling behaviour of the kurtosis parameter K as obtained directly from the data ($K_{\delta I_\alpha}$, open markers) or computed from the Castaing parameter ($K(\lambda_r^2)$, full markers), for the parallel (top panels) and perpendicular (bottom panels) directions. The horizontal line indicates the Gaussian reference value $K = 3$.

Table 1. Integral scale ℓ_α for parallel and perpendicular direction, for different values of ε^I

ε^I	$\ell_\perp[\mu m]$	$\ell_\parallel[\mu m]$
9.89	21	23
20.16	22	25
27.09	20	22
49.50	17	22
52.29	16	20

(left panels), where the Castaing model provides a slightly larger value of the kurtosis with respect to the direct estimate. This confirms the appropriateness of the representation of the PDFs obtained using the Castaing model [44].

The validation of the Castaing model [44] for EHD given in this section thus supports the framework of a nonlinear fragmentation process as responsible for the chaotic fields fluctuations, and the analogy between fluid turbulence and nonlinear EHD.

Structure Functions and Extended Self-Similarity in EHD Turbulence

An alternative way to describe the scaling variation of PDFs of the filed fluctuations is by observing the deviation of the structure function scaling exponents from the linear dependence on the order, typical of intermittency [3].

Structure functions are defined as the scale dependent pth-order moments of the PDFs. For a scalar field $v(x)$ and a scale r, they can be evaluated as $S_r^p(v) = \langle |v(x+r) - v(x)|^p \rangle$. Turbulent fields are characterized by power-law scaling of the structure functions within the inertial range, $S_r^p(v) \propto r^{\zeta_p}$. In case of homogeneous, isotropic, fully developed Navier-Stokes turbulence, scaling exponents can be predicted to be a linear function of the order, $\zeta_p = p/3$, if intermittency is not present. However, it is almost universally observed that intermittent corrections result in the deviation from such linear law [3].

In anisotropic EHD turbulence, the scaling behavior of the field $\delta_{r,\alpha} I(x)$ can be analyzed by introducing the parallel ($S^p_{r,\parallel}$) and perpendicular ($S^p_{r,\perp}$) structure functions (parallel and perpendicular refer as usual to the WD axis):

$$S^p_{r,\perp} = \left\langle \left|(I'(x, y+r) - I'(x, y)\right|^p \right\rangle$$
$$S^p_{r,\parallel} = \left\langle \left|(I'(x+r, y) - I'(x, y)\right|^p \right\rangle.$$

Intensity fluctuations at lags r in the range $2\pi\kappa_{max}^{-1} > r > 2\ell_\alpha$ are investigated here. κ_{max} is the largest resolved wave-vector and ℓ_α is the integral scale in the direction α (i.e.$\ell_\perp$,$\ell_\parallel$), defined as:

$$\ell_\alpha = \frac{\int_0^\infty |I'(\kappa_\alpha)|^2 \kappa_\alpha^{-1} d\kappa_\alpha}{\int_0^\infty |I'(\kappa_\alpha)|^2 d\kappa_\alpha}.$$

Values of ℓ_α obtained for our dataset are listed in Table 1. The integral scale slowly decreases with the voltage in both the perpendicular and parallel directions, as expected by mere observation of the samples.

One example of the parallel structure functions $S^p_{r,\parallel}$ is shown in figure 9 for the intensity fluctuations at $\varepsilon^I = 9.8$, and for moment orders up to $p = 5$. Note that larger order moments

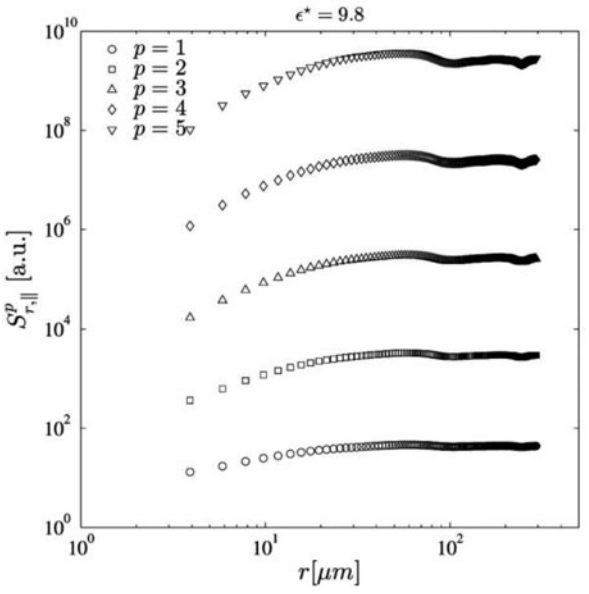

Figure 9A. One example of the parallel structure functions $S^p_{r,\parallel}$ *vs* the scale r, up to the fifth order ($p = 5$), computed for $\varepsilon^I = 9.8$, and expressed in arbitrary units.

are likely to be affected by severe statistical errors for our dataset size, so we discard them in this work. As expected because of the limited extension of the power-law range and of the presence of two separated scaling ranges, as observed in the spectra, the structure function do not show clear evidence of power-law scaling. A power-law fit can be however

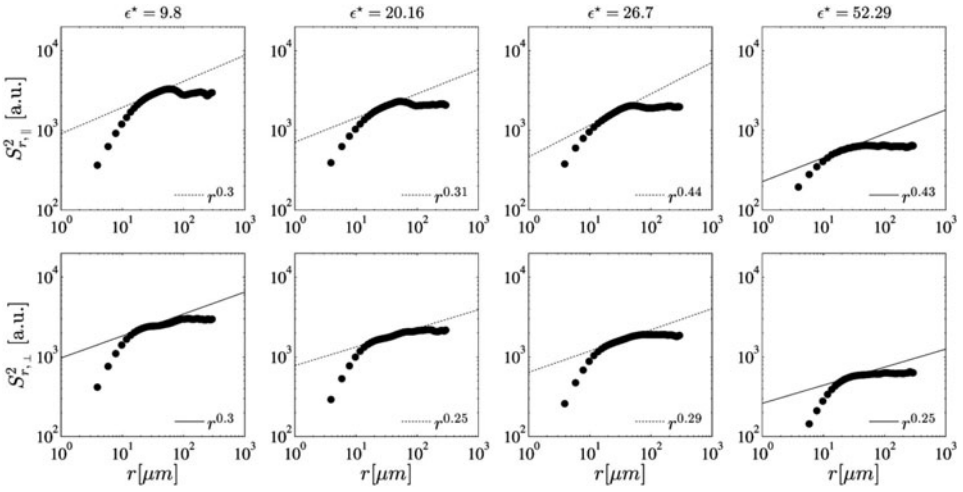

Figure 9B. Fit of the second-order structure functions $S^2_{r,\alpha}$ for the parallel (top panels) and perpendicular (bottom panels) fluctuations, at four different values of ε^I (see titles). The dotted lines represent power-law fits of the structure functions, while the full lines (bottom left and bottom right panels) are used as reference to guide the eye when no power-law fit could be performed.

attempted in a limited range of scale. Figure 9 shows such fit for the second order moment, for both parallel and perpendicular directions, and for four different regimes, as previously shown. The scaling exponents for all the five orders are collected in table 2, plotted in figure 11 (open markers), and will be discussed in the following.

In turbulence studies, Extended Self-Similarity (ESS) is often used to estimate relative scaling exponents [52–53]. ESS is a phenomenological result, which extends the validity of the power law scaling outside the inertial range, or even to cases where power law scaling is not clearly observed (e.g. at low Reynolds number). This allows the evaluation of the scaling exponents, and therefore of the intermittency effects, even for data with poorly defined inertial range, such as in the case under study. Therefore, we perform ESS in order to test the quality of the structure functions fits, and to verify its validity in this system.

Although ESS is not based upon explicit theoretical hypotheses, in most cases it is related with the linear scaling of the structure functions of some specific order (depending on the system, as for example the third order moment for fully developed homogeneous, isotropic Navier-Stokes turbulence, for which a theoretical prescription holds [3]).

Theoretical attempts to justify the ESS general approach have been discussed [54].

Unlike fully developed Navier-Stokes turbulence, in EHD there is no theoretical prescription for the third order moment (nor any other) scaling. In such cases, it is still possible to apply ESS if an independent estimate of the scaling exponent can be recovered for one of the moments. Since the spectral slope β is simply related to the second order structure function scaling exponent through $\zeta_2 = \beta - 1$, it is possible to use the power-law fit of the spectrum to indirectly obtain ζ_2. This parameter (and therefore the second order structure function) can then be used as reference for ESS. Note that the second order scaling exponents obtained from the fit of the structure function are fully compatible with the values obtained from the spectral indices (cf. Table 2 and fig. 9).

Based on these qualitative analogies, we make use of ESS to describe the intermittency in the system under study. We assume here that scaling exponents estimated using ESS, which we label $\hat{\zeta}_{p,\alpha}$, are a reasonable proxy of the real exponents. In fact, as described in [54], $S^p_{r,\alpha} \sim (S^2_{r,\alpha})\xi_{p,2}$ to $\xi_{p=2,\alpha} = \hat{\zeta}_{p,\alpha}/\zeta_{2,\alpha}$ and α represents the parallel or perpendicular direction. Thus the scaling exponents are simply obtained as $\hat{\zeta}_{p,\alpha} = \xi_{p,2}$ to $\xi_{p=2,\alpha}\,\zeta_{2,\alpha}$.

In figure 10, examples of structure functions are plotted in the ESS representation, as a function of the second order $S^2_{r,\|}$. The relative structure functions are now clear power laws $S^p_{r,\alpha} \propto S^{2^{\xi_{p,\alpha}}}_{r,\|}$, over the whole range, for all orders p, and for all regimes (not shown).

The relative scaling exponents $\hat{\zeta}_{p,\alpha}$, evaluated by fitting the structure functions assuming ESS, are plotted in figure 11 (full markers), along with the scaling exponents obtained through direct fit of the structure functions (open markers, see table 2). The straight lines are the non-intermittent prediction from the experimental spectral indices, $\zeta_{p,\alpha} = p(\beta - 1)/2$.

Note that direct fit of the structure functions was not possible in the $\varepsilon^I = 9.8$ regime for the perpendicular fluctuations, due to the poor scaling. In all the other cases, a very good agreement is observed between the exponents computed directly from the data and with ESS. This important result shows the validity of ESS in the EHD samples, confirming both the appropriateness of the study of EHD in the framework of turbulence, and supporting the universal validity of ESS.

A significant departure from the linear dependence of the scaling exponents on the order can be observed for voltages up to the onset of the DSM2 mode, $\varepsilon^I < 52.29$, resembling the typical behaviour of intermittent fluid turbulence.

The observed departure is more important for parallel structure functions. The difference between parallel and perpendicular directions could be connected to the

Table 2. Scaling exponents ζ_α of the $n-$ th order structure functions for parallel and perpendicular direction, at four different values of ε^I

	$\varepsilon^I = 9.8$		$\varepsilon^I = 20.16$		$\varepsilon^I = 26.7$		$\varepsilon^I = 52.29$	
P	$\zeta_\parallel$	$\zeta_\perp$	$\zeta_\parallel$	$\zeta_\perp$	$\zeta_\parallel$	$\zeta_\perp$	$\zeta_\parallel$	$\zeta_\perp$
1	0.21 ± 0.01	—	0.22 ± 0.01	0.15 ± 0.02	0.26 ± 0.01	0.24 ± 0.03	0.14 ± 0.03	0.17 ± 0.04
2	0.30 ± 0.01	—	0.31 ± 0.01	0.23 ± 0.03	0.44 ± 0.01	0.31 ± 0.01	0.22 ± 0.04	0.25 ± 0.05
3	0.37 ± 0.03	—	0.46 ± 0.03	0.31 ± 0.03	0.65 ± 0.02	0.42 ± 0.04	0.38 ± 0.04	0.41 ± 0.05
4	0.44 ± 0.03	—	0.52 ± 0.03	0.43 ± 0.07	0.77 ± 0.03	0.52 ± 0.04	0.45 ± 0.04	0.50 ± 0.05
5	0.54 ± 0.04	—	0.62 ± 0.05	0.48 ± 0.10	0.83 ± 0.04	0.60 ± 0.05	0.57 ± 0.05	0.56 ± 0.07

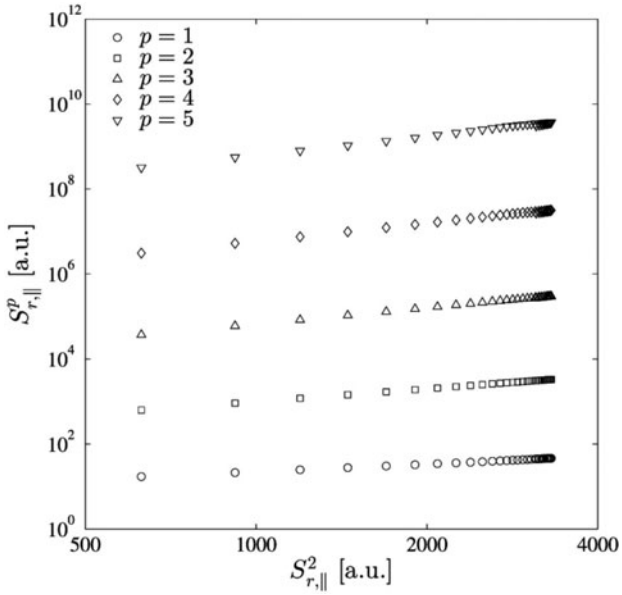

Figure 10. Examples of structure functions $S^p_{r,\parallel}$ *vs* $S^2_{r,\parallel}$ for parallel direction, and $\varepsilon^I = 9.8$, in arbitrary units.

aforementioned presence of the sweeping effect, due to large scale coherent structures, as recently observed in the parallel direction [28], which highlights the anisotropic nature of the fluctuations.

Finally, the ESS analysis of the DSM2 regime confirms that weaker intermittency is present. The scaling exponents deviation from the linear prediction is less evident than

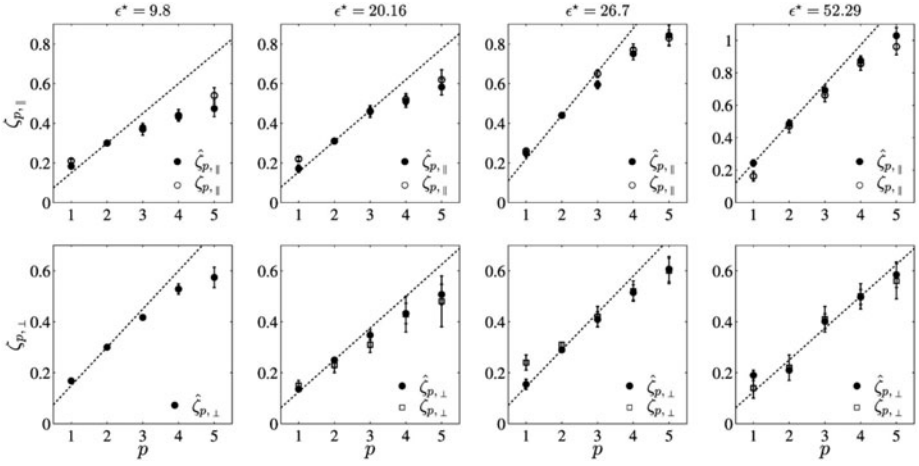

Figure 11. The scaling exponents $\zeta_{p,\parallel}$ and $\zeta_{p,\perp}$ for different values of ε^I(full markers, see legend), as obtained from direct fit of the structure functions (open symbols, see Table 2) and from ESS (full symbols). The straight lines show the non-intermittent prediction obtained from the spectra, $\zeta_{p,\alpha} = p(\beta - 1)/2$.

in the other regimes, again in agreement with the other quantities presented in previous Section. This is particularly evident in the perpendicular direction.

Conclusions

Motivated by the qualitative analogy between the turbulent motion of fluids and the chaotic dynamics of electroconvection, we have studied the statistical properties of different regimes of EHD instabilities in NLC, through the analysis of intensity fluctuations PDFs and structure functions. In order to account for the persistent anisotropy arising from the sample properties, light intensity fluctuations have been considered separately in the directions parallel and perpendicular to the axis of the William Domains convective rolls, which set up at low voltage.

Spectral analysis has shown scaling laws, which supports the presence of a fragmentation process similar to fluid turbulence. This has been observed starting at intermediate voltage, in the so called "weak turbulence" regime, and at higher voltage regimes. Spectral indices, and the extension of the scaling range have confirmed the anisotropic character of the fluctuations, indicating a more developed spectrum for parallel fluctuations.

The scale dependent PDFs of the field fluctuations indicated intermittent fluctuations. PDFs have been satisfactorily modeled using the Castaing approach, and the quantitative intermittency parameter λ_r^2 has been estimated. The validation of the Castaing model also supports the multifractal nature of the fluctuations, as further evidenced by the kurtosis scaling law. These results have confirmed again the possible presence of a turbulent-like fragmentation process, and that differences exist between the parallel and perpendicular directions. In particular, the parallel direction has shown stronger intermittency (seen as departure from Gaussian PDF), except in the highly chaotic DSM2 regime, where intermittecy seems to reduce considerably and isotropize. Incidentally, the observation of anisotropic intermittency might be connected with the results of previous studies of spatio-temporal decorrelation in a similar system, which provided evidence of sweeping effect setting up at low voltage only in the parallel direction. However, further studies would be needed to identify the mechanism responsible for such behaviour.

The study of the structure functions scaling exponents has shown that ESS applies to EHD. This supports once more the appropriateness of the turbulence framework for the description of EHD fluctuations, and of the use of the corresponding tools. Moreover, it confirms the importance and universality of ESS as tool for turbulence studies, for samples where the inertial range is not well defined. ESS analysis has confirmed the results obtained through the study of the PDFs, including the anisotropic features.

The smooth transition across several EHD regimes has been thus characterized, showing striking similarity with fluid turbulence, the presence of intermittency, and the importance of anisotropy. The latter may be connected with the anisotropy of the sweeping effect, which was previously observed only along the WD axis.

The results obtained here confirm the relevance of a fragmentation process underlying the increasing presence of small scale fluctuations for increasing voltage, and stimulate further theoretical efforts for the description of EHD complex dynamics in the framework of fully developed turbulence.

References

[1] Monin, A. S. & Yaglom, A. M. (2007). *Statistical Fluid Mechanics: Mechanics of Turbulence*, Dover, New York.

[2] McComb, W. D., (1990). *The physics of fluid turbulence*, Oxford Univ. Press, New York
[3] Frisch, U., (1995). *Turbulence: the legacy of A. N. Kolmogorov*, Cambridge Univ. Press, Cambridge UK.
[4] Sreenivasan, K. R., (1985). *J. Fluid Mech. 151*, 81.
[5] Sreenivasan, K. R. & Antonia, R. A., (1997). *Ann. Rev. Fluid Mech. 29*, 435.
[6] Anselmet, F. *et al.*, (1984). *J. Fluid Mech. 140*, 63.
[7] Arneodo, A. *et al.*, (1996). *Europhys. Lett. 34*, 411.
[8] Vincent, A. & Meneguzzi, M., (1991). *J. Fluid Mech. 225*, 1.
[9] Boratav, O. N. & Pelz, R. B., (1997). *Phys. Fluids 9*, 1400.
[10] Kolmogorov, A. N., (1941). *C. R. Acad. Sci. U.R.S.S. 36*, 301.
[11] Bruno, R. & Carbone, V., (2005). *Liv. Rev. Sol. Phys. 2*, 4.
[12] Burlaga, L., (1991). *J. Geophys. Res. 96*, 5847.
[13] Marsch, E. & Tu, C.-Y., (1997). *Nlin. Proc. Geophys. 4*, 101.
[14] Carbone, V., (1993). *Phys. Rev. Lett. 71*, 1546.
[15] Politano, H., Pouquet, A., & Carbone, V., (1998). *Europhys. Lett.*, *43*, 516.
[16] Camussi, R. *et al.*, (1996). *Phys. Fluids*, *8*, 1181.
[17] Noullez, A. *et al.*, (1997). *J. Fluid Mech. 339*, 287.
[18] Protas, B., Goujon-Durand, S. & Wesfreid, J. E., (1997) *Phys. Rev. E*, *55*, 4165.
[19] Gaudin, E. *et al.*, (1998). *Phys. Rev. E*, *57*, R9.
[20] Biferale & Procaccia, (2005). *Phys. Rep.*, *414*, 43
[21] De Gennes, P. G., (1993). *The Physics of Liquid Crystals*, Oxford Science Pub., Oxford UK.
[22] Blinov, L. M., (1983). *Electro-Optical and Magneto-Optical properties of Liquid Crystals*, Wiley, New York
[23] Joets, A. & Ribotta, R., (1986). *J. Phys. (Paris)*, *47*, 595.
[24] Cross, M. C. & Hohenberg, P. C., (1993). *Rev. Mod. Phys.*, *65*, 851.
[25] Kai, S. *et al.*, (1975). *J. Phys. Soc. Jpn.*, *38*, 1789.
[26] Carbone, F. *et al.*, (2010). *Europhys. Lett.*, *89*, 46004.
[27] Carbone, F., Vecchio, A. & Sorriso-Valvo, L., (2011). *Eur. Phys. J. E*, *34*, 75.
[28] Carbone, F. *et al.*, (2011). *Phys. Rev. Lett. 106*, 114502.
[29] Daya, Z. A., Deyirmenjian, V. B., Morris, S. W., & de Bruyn, J. R. (1998). *Phys. Rev. Lett.*, *80*, 964.
[30] Daya, Z. A., Deyirmenjian, V. B., & Morris, S. W., (1999). *Physics of Fluids (1994-present) 11*, 3613.
[31] Deyirmenjian, V. B., Daya, Z. A., and Morris, S. W., (2005). *Physical Review E*, *72*, 036211.
[32] Strangi, G., Ferjani, S., Barna, V., De Luca, A., Versace, C., Scaramuzza, N., and Bartolino, R., (2006). *Opt. Exp.*, *14*, 7737.
[33] Ferjani, S., Sorriso-Valvo, L., De Luca, A., Barna, V., De Marco, R., and Strangi, G., (2008) *Phys. Rev. E*, *78*, 011707.
[34] Shiyanovskii, S. V., Smalyukh, I. I., & Lavrentovich, O. D., (2001) *Computer simulations and fluorescence confocal polarizing microscopy of structures in cholesteric liquid crystals*, Kluwer Academic Publishers: The Netherlands.
[35] Smalyukh, I., Pratiba, R., Madhustudana, N. V., & Lavrentovich, O. D., (2005). *Euro. Phys. J. E*, *16*, 179.
[36] Zappone, B. *et al.*, (2012). *Soft Matter*, *8*, 4318.
[37] Ericksen, J. L., (1959). *Arch. Ration. Mech. Anal.*, *4*, 231.
[38] Leslie, F. M., (1968). *Arch. Ration. Mech. Anal.*, *28*, 265.
[39] Parodi, O., (1970). *Le Journal de Physique*, *31*, 581.
[40] Te-Sheng, L. et. al, (2013). *Physics of Fluids*, *2*, 082102.
[41] Chandrasekhar, S., (1982). *Hydrodynamic and Hydromagnetic Stability*, Dover.
[42] Carbone, V., Versace, C. & Scaramuzza, N., (1997). *Physica D*, *106*, 314.
[43] Takeuchi, K. A., Kuroda, M., Chaté, H., and Sano, M., (2007). *Phys. Rev. Lett.*, *99*, 234503.
[44] Castaing, B., Gagne, Y., & Hopfinger, V., (1990). *Physica D*, *46*, 177.
[45] Marsch, E., & Tu, C.-Y., (1994). *Ann. Geophys.*, *12*, 1127.

[46] Sorriso-Valvo, L. *et al.*, (1999). *Geophys. Res. Lett.*, *26*, 1804.
[47] Sorriso-Valvo, L. L. *et al.*, (2000). *Europhys. Lett.*, *51*, 520.
[48] Sorriso-Valvo, L. *et al.*, (2001). *Plan. Space Sci. 49*, 1193.
[49] Sorriso-Valvo, L., Carbone, V. & Bruno, R., (2004). *Europhys. Lett.*, *67*, 504.
[50] Carbone, V. *et al.*, (2005). *Riv. Nuovo Cimento*, *27*, 1.
[51] Kolmogorov, A. N., (1962). *J. Fluid Mech.*, *13*, 82.
[52] Benzi, R. *et al.*, (1993). *Phys. Rev. E*, *48*, 29.
[53] Benzi, R. *et al.*, (1996). *Physica D*, *96*, 162.
[54] Ruiz-Chavarria, G., Baudet, C., & Ciliberto, S., (1996). *Physica D*, *99*, 369.